Eleventh U.S. National Conference on Earthquake Engineering
Integrating Science, Engineering & Policy
June 25-29, 2018
Los Angeles, California

FLEXURAL COMPRESSION CAPACITY OF THIN REINFORCED CONCRETE STRUCTURAL WALLS

C.L. Segura[1] , C.A. Arteta[2], G. Araujo[3]
and J.W. Wallace[4]

ABSTRACT

Stability of slender reinforced concrete walls has become an issue of interest for researchers since observations of their performance in recent earthquakes indicated that code compliant walls may be vulnerable to brittle compression failure and rebar buckling prior to achieving code-allowable drift limits. To understand the issues that led to poor performance of these walls, researchers have conducted tests on code-compliant wall specimens. To test the compressive strain limits at the edge of the walls, some of these tests have been conducted on isolated boundary elements with uniform compressive loading (zero curvature), which is a more economical approach than tests on full wall specimens. To analyze the influence of curvature in predicted flexural compression capacity, two code compliant walls were subjected to combined axial load and reversed cyclic lateral loading, and three rectangular boundary element specimens, representative of the confined compression region of a wall, were subjected to monotonic compression to failure. Results from this small set of experimental data were used to estimate a relationship between compression strain capacity (at the extreme compression fiber) and strain gradient. The results suggest that isolated boundary element tests define a lower bound of the actual compressive strain limits to predict the flexural compression capacity of a wall under cyclic loading.

[1]Reasearch Structural Engineer, National Institute of Standards and Technology, Gaithersburg, MD 20899 (email: christopher.segura@nist.gov)
[2]Assistant Professor, Dept. of Civil and Environmental Engineering, Universidad del Norte, Barranquilla. Colombia.
[3]Graduate Student Researcher, Dept. of Civil and Environmental Engineering, Universidad del Norte, Barranquilla. Colombia.
[4]Professor, University of California, Los Angeles, Los Angeles, CA 90095.

Segura, C.L., Arteta, C.A., Araujo, G., and Wallace, J.W. Flexural compression capacity of thin reinforced concrete structural walls. *Proceedings of the 11th National Conference in Earthquake Engineering*, Earthquake Engineering Research Institute, Los Angeles, CA. 2018.

Flexural Compression Capacity of Thin Reinforced Concrete Structural Walls

C.L. Segura[1], C.A. Arteta[2], G. Araujo[3]
and J.W. Wallace[4]

ABSTRACT

Stability of slender reinforced concrete walls has become an issue of interest for researchers since observations of their performance in recent earthquakes indicated that code compliant walls may be vulnerable to brittle compression failure and rebar buckling prior to achieving code-allowable drift limits. To understand the issues that led to poor performance of these walls, researchers have conducted tests on code-compliant wall specimens. To test the compressive strain limits at the edge of the walls, some of these tests have been conducted on isolated boundary elements with uniform compressive loading (zero curvature), which is a more economical approach than tests on full wall specimens. To analyze the influence of curvature in predicted flexural compression capacity, two code compliant walls were subjected to combined axial load and reversed cyclic lateral loading, and three rectangular boundary element specimens, representative of the confined compression region of a wall, were subjected to monotonic compression to failure. Results from this small set of experimental data were used to estimate a relationship between compression strain capacity (at the extreme compression fiber) and strain gradient. The results suggest that isolated boundary element tests define a lower bound of the actual compressive strain limits to predict the flexural compression capacity of a wall under cyclic loading.

Introduction

Observations of slender reinforced concrete walls following recent earthquakes in Chile and New Zealand has led to several studies focused on understanding the reasons for poor performance of these walls [e.g., 1, 2]. Experimental work has been conducted on isolated boundary elements subjected to either monotonic compression [3] or cyclic tension and compression [4, 5]. For these tests, uniform axial strain is applied to the specimens (Fig. 1a) to simulate the flexural (axial) demands within the plastic hinge region of a wall. Stress-strain data from isolated boundary element tests are often used to calibrate models to predict the flexural behavior and lateral drift capacity of walls. Predicting the drift capacity of a wall using such data may be considered a worst-case scenario because the flexural response of a wall results in a strain gradient (Fig. 1b) as compared to the uniform strain condition applied to isolated boundary elements (Fig. 1a).

[1]Reasearch Structural Engineer, National Institute of Standards and Technology, Gaithersburg, MD 20899 (email: christopher.segura@nist.gov)
[2]Assistant Professor, Dept. of Civil and Environmental Engineering, Universidad del Norte, Barranquilla. Colombia.
[3]Graduate Student Researcher, Dept. of Civil and Environmental Engineering, Universidad del Norte, Barranquilla. Colombia.
[4]Professor, University of California, Los Angeles, Los Angeles, CA 90095.

Segura, C.L., Arteta, C.A., Araujo, G., and Wallace, J.W. Flexural compression capacity of thin reinforced concrete structural walls. *Proceedings of the 11th National Conference in Earthquake Engineering*, Earthquake Engineering Research Institute, Los Angeles, CA. 2018.

Recent laboratory tests have also been conducted on wall panel specimens constructed with geometry and boundary transverse reinforcement similar to recent isolated boundary element tests [1], enabling a direct comparison between wall and boundary element results. In this paper, the compressive deformation capacity (i.e., strain capacity) of recent boundary element tests is compared to that of recent wall panel tests to better understand how boundary element test results may be used to predict the flexural behavior of walls.

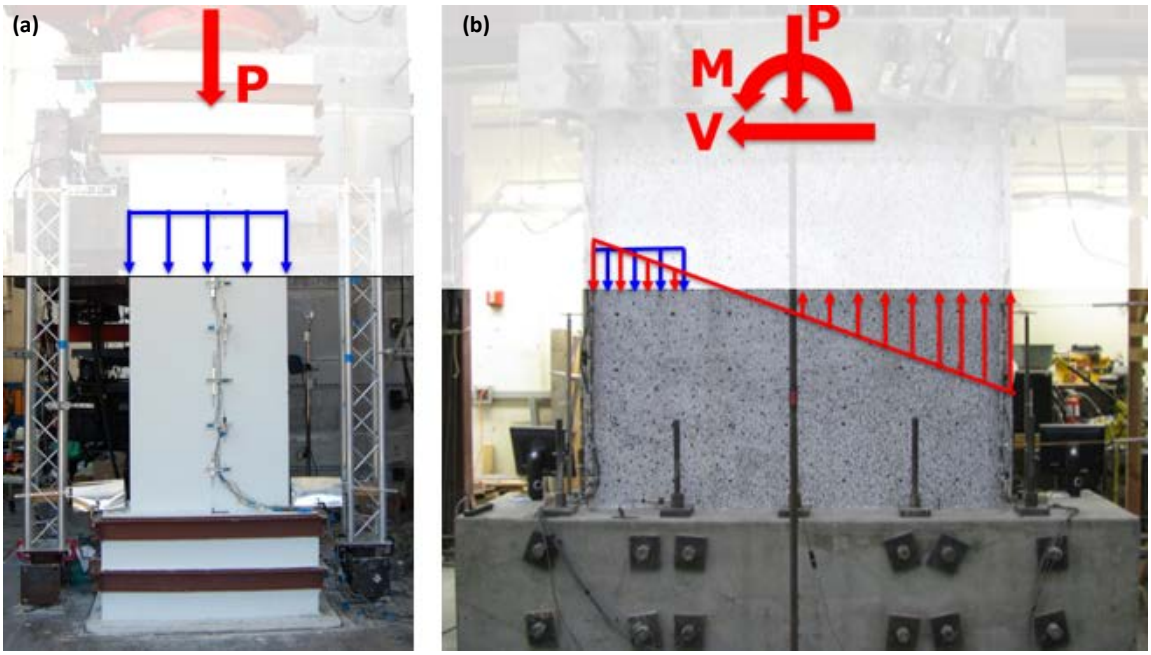

Figure 1. Loading conditions on (a) isolated boundary element; and (b) wall panel

Description of Laboratory Test Specimens

Experimental findings are presented in this paper for three boundary element specimens (designated W7, W9, and W11) that represent the confined boundary region of a wall, and two half-scale wall panel specimens (designated WP1 and WP4) that represent approximately the bottom 1.5 stories of an eight-story cantilever wall. Fig. 2a shows the test setup used to apply loads to the boundary element specimens. A 4-million-pound universal testing machine applied increasing monotonic displacements to the top of the specimen to produce the uniform strain conditions shown in Fig. 1a. The test setup used for the wall panel specimens is shown in Fig. 2b. Increasing cyclic wall rotations were imposed using two vertically-aligned actuators and one horizontally-aligned actuator. The applied loading pattern simulated the axial load, shear force, and overturning moment demand expected in the lower portion of an eight-story cantilever wall.

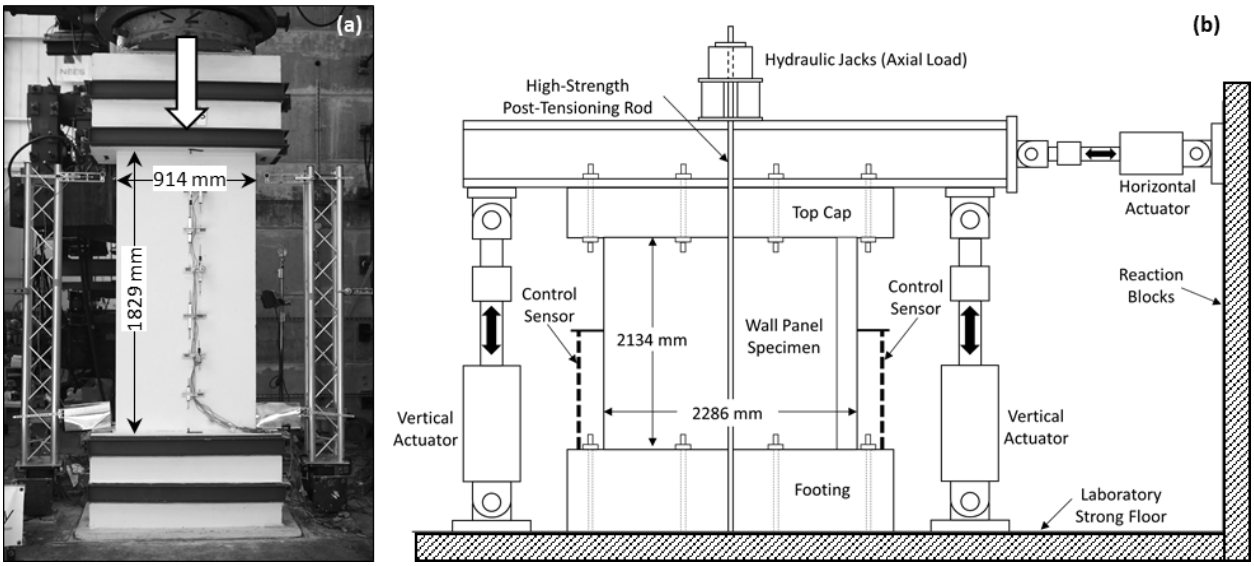

Figure 2. Test setup for (a) isolated boundary element test; and (b) wall panel test

Cross-sectional geometries and reinforcement details are shown in Fig. 3 for all five test specimens. Specified concrete strength was f'_c = 28 MPa for the isolated boundary elements and f'_c = 35 MPa for the wall panel specimens. Specified yield strength was f_y = 414 MPa for all reinforcing steel. For the wall panel specimens, 6.4 mm and 8.1 mm diameter ASTM A1064 deformed wire [6] was used for boundary transverse reinforcement. All other reinforcement was ASTM A706/A615 [7] Grade 60 deformed bar. The full-scale isolated boundary element specimens were 305 mm thick and 914 mm wide. The quantity and configuration of transverse reinforcement for the three boundary element specimens satisfied ACI 318-11 special boundary element provisions [8], and one specimen (W9) also satisfied the more stringent requirements of ACI 318-14 [9]. The approximately one-half scale wall panel specimens were 152 mm thick and 2286 mm in length, and the quantity and configuration of boundary transverse reinforcement satisfied ACI 318-11 and 318-14 provisions. For both walls, an axial load equal to 10% of the nominal compressive strength of the wall web ($P_u = 0.10A_{cv}f'_c$, where A_{cv} is the gross area bounded by the wall web and wall length) was held constant throughout the test. The confined boundary regions of WP1 extended 356 mm from the wall edges, which was approximately 1.2 times the confined length required by ACI 318-14. Longitudinal reinforcement was different in the two boundaries of WP1 to compare the behavior of configurations in which all longitudinal bars are laterally restrained by hoops or crossties to those in which every other bar is laterally restrained (Fig. 3b). For specimen WP4, a longer confinement depth was required at the thin (web) boundary because of the increased compression depth imposed as a result of the larger quantity of tension steel (14 ∅19.1 mm in the flange boundary) as compared to WP1. The confined boundary of specimen WP4 extended 457 mm from the edge of the wall, making it a one-half scale representation of specimen W11.

Photos of typical damage to an isolated boundary element specimen and a wall panel specimen are shown in Fig. 4a and Fig. 4b, respectively. Brittle compression failures were observed for each of the boundary element specimens with damage characterized by buckling of longitudinal reinforcement and crushing of confined core concrete, regardless of whether or not lateral support

was provided by crossties. Damage to core concrete and buckling of longitudinal reinforcement generally concentrated within a height of approximately 2.5 times the thickness of the specimens (i.e., 2.5*b*). Similarly, brittle flexure-compression failure modes (boundary and web crushing and rebar buckling) were observed at the boundaries of each of the wall panels with damage occurring over a height of about 2.5*b*. It is noteworthy that buckling of longitudinal reinforcement was observed in all boundary element and wall panel specimens even though the ratio of transverse reinforcement spacing to longitudinal bar diameter (s/d_b) was between 3.2 and 4.0, which is smaller than the $s/d_b \leq 6$ limit imposed by ACI 318-14.

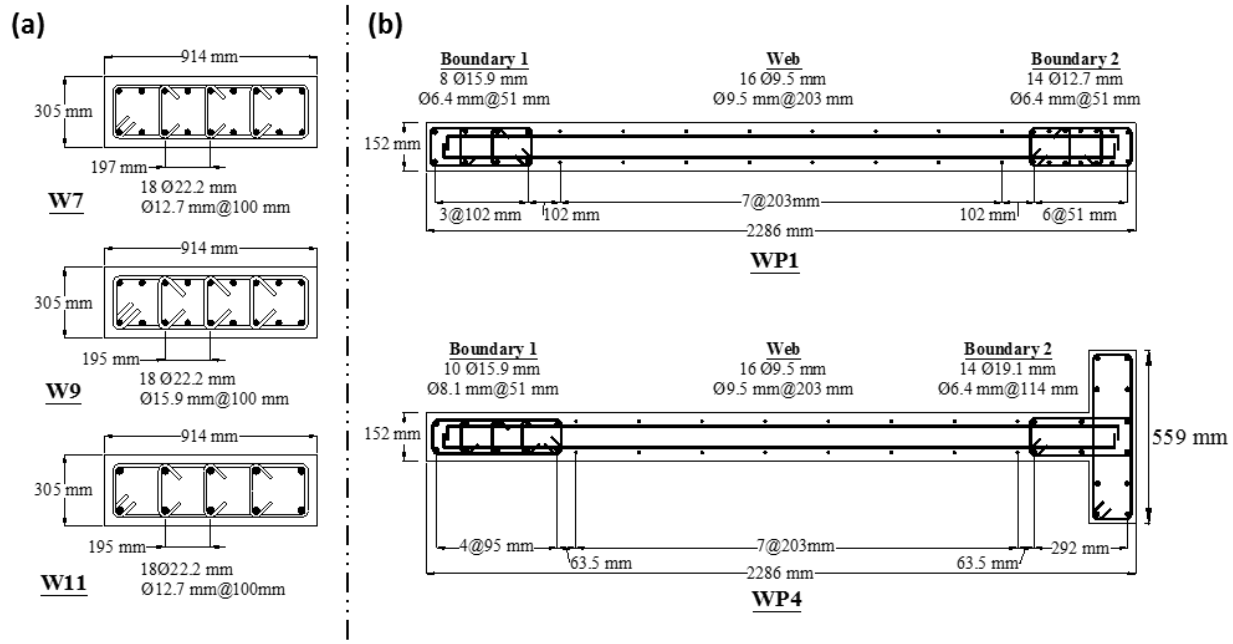

Figure 3. Cross-sectional geometry and reinforcement for (a) isolated boundary element specimens; and (b) wall panel specimens. Note: 1 in. = 25.4 mm.

Test Results and Observations

A typical normalized axial force vs. strain response is shown in Fig. 5a for boundary element specimen W11. The reported axial load is normalized to the nominal compression capacity of the specimen ($P_0 = 0.85f_c'(A_g - A_{st}) + f_y A_{st}$, where A_g is the gross cross-sectional area and A_{st} is the total cross-sectional area of longitudinal reinforcement). The global average strain was calculated by dividing the measured shortening by the specimen height. The height over which concrete crushing and rebar buckling damage were observed (L_{DZ}) is reported in Table 1 for the three specimens. The damaged zone strain in Fig. 5 is the average strain measured over L_{DZ}, which was approximately equal to 2.5 times the wall thickness for each specimen (see Fig. 4a). Also shown in Fig. 5b is the inferred core stress (axial force resisted by confined concrete divided by core area) vs. damaged zone axial strain, measured over a gage length of 2.5*b*. An analytical stress-strain curve for confined concrete according to the equations proposed by Mander et al. [10] is also shown. Table 1 provides test results for each of the specimens, including the observed damaged zone length normalized to wall thickness (L_{DZ}/b) and the measured strain (assuming a gage length of 2.5*b*) corresponding to a 20% reduction in strength (ε_{cu}). Measured strains at strength loss ranged between 0.008 and 0.013. The confined concrete compression fracture energy

(G_f^{cc}) reported in Table 1 was calculated as the area under the inelastic portion of the core stress vs. strain response, as denoted by the yellow shaded region in Fig. 5b. This value may be used to calibrate confined concrete properties for analytical models [4,5]. Measured $[G_f^{cc}, L_{DZ}]$ pairs are W7=[455,841], W9=[490,936], W11=[365,863], where G_f^{cc} is in N/mm and L_{DZ} in mm. There is some variability in measured G_f^{cc} values even though the quantity and arrangement of reinforcement was relatively similar for the three boundary element specimens.

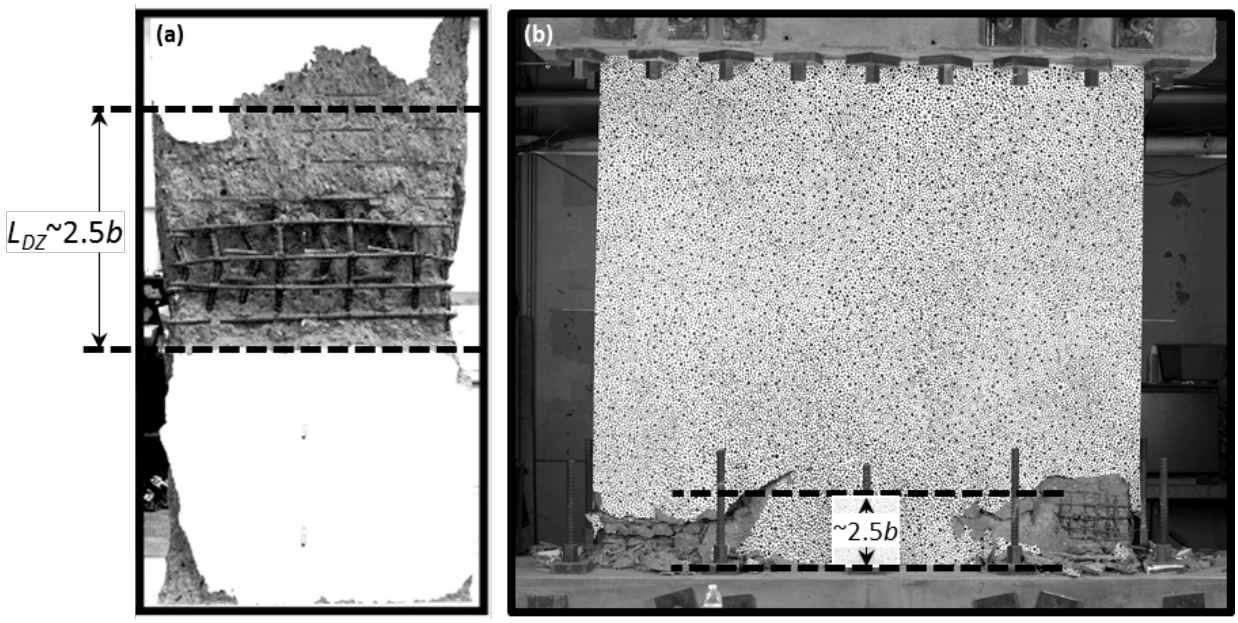

Figure 4. (a) Photo of boundary element specimen W7 taken at end of test showing damage concentrated primarily over a height 2.5 times the wall thickness; and (b) photo of wall panel specimen WP1 taken at end of test showing damage at boundaries concentrated over a height of 2.5 times the wall thickness.

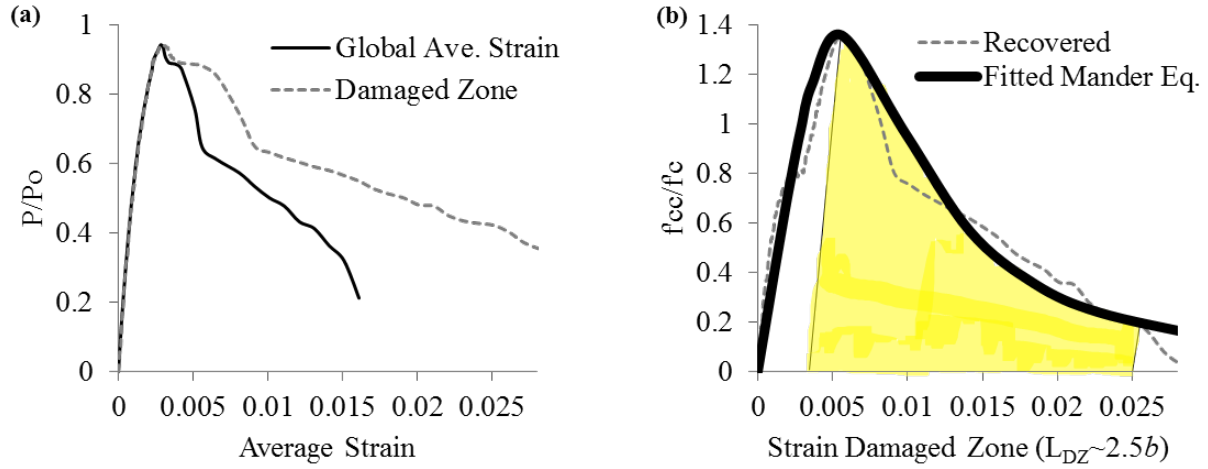

Figure 5. Isolated boundary element test results: (a) Typical force-strain response; and (b) recovered core experimental stress-strain response.

Table 1. Observed parameters of isolated boundary element tests

Parameter	W7	W9	W11
L_{DZ}/b	2.75	3.06	2.83
ε_{cu}	0.013	0.011	0.008
G_f^{cc} [N/mm]	455	490	365

Note: 175.1 N/mm = 1 Kips/in.

Fig. 6a presents the normalized measured base moment vs. hinge rotation for the two wall panel specimens. Hinge rotation was measured over an assumed hinge length of one-half the length of the wall ($l_w/2$) using two vertically-aligned control sensors mounted at opposite ends of the wall (Fig. 2b). Rotation measurements are presented rather than wall lateral drift because hinge rotation is directly related to flexural deformations, which is the focus of this study. For specimen WP1, initial strength loss occurred prior to reaching +1.5% rotation at which time crushing of confined concrete and buckling of longitudinal reinforcement was observed at the wall boundary constructed with 8 ∅15.9 mm longitudinal reinforcing bars (Fig. 4b). In the following loading cycle, out-of-plane instability of the previously damaged boundary region occurred, and the wall demonstrated very little residual strength in the positive loading direction. While loading monotonically in the opposite direction, abrupt crushing of the opposite boundary (14 ∅12.7 mm longitudinal bars) occurred (Fig. 4b) at -1.97% rotation and lateral strength immediately dropped to approximately 40% of the peak strength measured in previous cycles. For WP4, crushing of the confined boundary, extending into the unconfined web region of the wall, was observed at +1.3% rotation, with an immediate drop in lateral strength. Axial strain profiles measured at strength loss are shown in Fig. 6b for each wall. The reported axial strains were measured over a gage length of 2.5*b*, the height over which compression damage was observed at the boundaries of the walls. As indicated in Fig. 6b, extreme fiber compression strains at strength loss ranged between 0.022 and 0.026, which is approximately 2 to 3 times the uniform strains measured for the boundary element specimens at strength loss ($0.008 \leq \varepsilon_{cu,80} \leq 0.013$). In fact, prior to strength loss, compression strains were generally greater than 0.01 over the entire confined boundary regions of the walls (356 mm from wall edges for WP1 and 457 mm from wall edge for WP4).

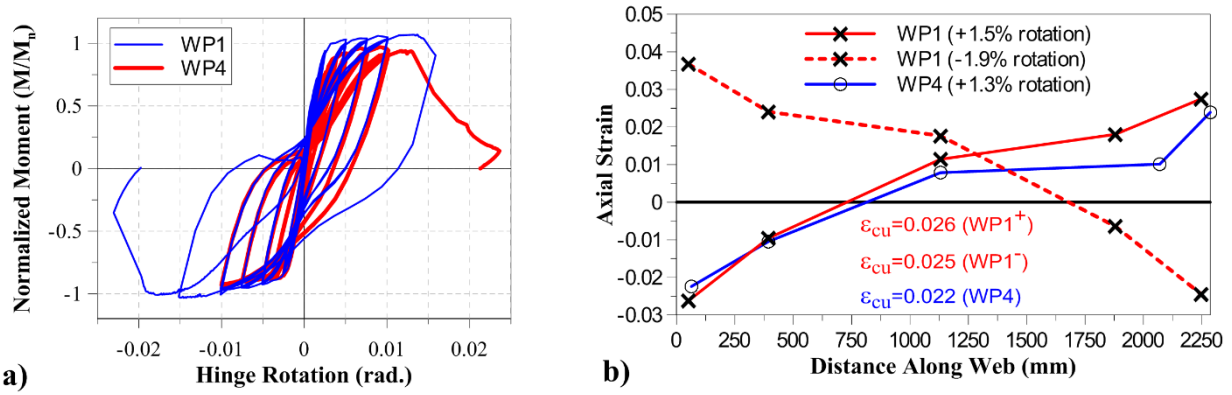

Figure 6. Wall panel test results: (a) Moment normalized by nominal flexural strengthvs. hinge rotation measured over assumed hinge length of $l_w/2$; and (b) Axial strain profiles measured over a gage length of 2.5*b*.

The primary difference between the confined region of the walls and the isolated boundary element specimens is the presence of a strain gradient (i.e., curvature) across the width of the confined region. In Fig. 7, the dependence of compression strain capacity upon curvature, calculated as the extreme fiber compression strain divided by the compression depth (i.e., ε_{cu}/c), is demonstrated. For the isolated boundary elements (W7, W9, and W11), curvature is assumed to be zero because the strain distribution is uniform. For the small sample size, a nearly linear relationship between curvature and strain capacity is apparent. The trend suggests that compression strain capacity of a wall decreases as the curvature demand necessary to reach that level of strain decreases. That is, as the strain distribution along the compression zone becomes more uniform, strain capacity becomes smaller.

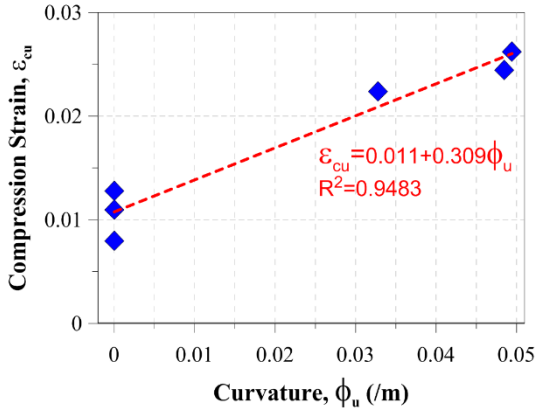

Figure 7. Comparison of compression strain measurements, as a function of curvature, from isolated boundary element tests (uniform strain) and wall panel tests (strain gradient)

Fig. 8a demonstrates the flexural response of a wall which is dominated by plastic rotation within the plastic hinge region. Wall flexural deformations can be expressed by the plastic hinge formulation given in Eq. 1, in which roof lateral displacement (δ_u) is determined as the sum of elastic displacement (δ_y) and inelastic displacement (δ_p). The inelastic displacement is assumed to occur as rigid plastic rotation (θ_p) centered at mid-height of the plastic hinge (i.e., $l_p/2$). Plastic rotation can be related to curvature at the section level according Eq. 2. At large lateral drift demands, elastic drift is relatively small in comparison to inelastic drift, and Eq. 1 can be simplified to Eq. 3. Based on Eq. 3, analytical strain profiles can be determined for a given roof drift demand (δ_u/h_w).

$$\delta_u = \delta_y + \delta_p = \delta_y + \theta_p\left(h_w - \frac{l_p}{2}\right) \quad (1)$$

$$\theta_p \approx \phi_p l_p \quad (2)$$

$$\frac{\delta_u}{h_w} \approx \theta_p \approx \phi_p l_p = \frac{\varepsilon_{cu}}{c} l_p \quad (3)$$

Fig. 8b explores the implications of the trend shown in Fig. 7 for two walls with different compression depth (influenced by longitudinal reinforcement, axial load, and cross-section shape).

Strain profiles for two walls, one with moderate compression depth (c_1) and another with large compression depth (c_2), are shown. For a given extreme fiber compression strain demand, the curvature demand for Wall 2, with $c = c_2$, is smaller than that of Wall 1, and the compression distribution is more uniform. If the compression strain capacity of the two walls is equal (i.e., $\varepsilon_{cu1} = \varepsilon_{cu2}$), the plastic rotation capacity of Wall 2 will be smaller than that of Wall 1 since plastic curvature and plastic rotation are directly related (i.e., Eq. 3). However, based on the trend suggested in Fig. 7, Wall 2 is likely to possess smaller compression strain capacity (i.e., $\varepsilon_{cu2} < \varepsilon_{cu1}$) because its curvature demand will be smaller for a given extreme fiber compression strain. As a result, the rotation and drift capacity of a wall designed for relatively large compression depth (Wall 2) may be significantly smaller than that of a wall with smaller compression depth demands. This is of particular importance because the lateral drift limits in ASCE 7 do not account for wall compression depth or curvature demand. Furthermore, a limit on compression strain or compression depth is not imposed in current building codes (i.e., ASCE 7 and ACI 318). This topic is the focus of ongoing work. A larger dataset is being compiled to study the compressive capacity of isolated boundary elements and walls on a larger scale. An analytical study is being conducted in parallel to compare the analytical results predicted by models utilizing constitutive modeling parameters derived from isolated boundary element tests to wall test results.

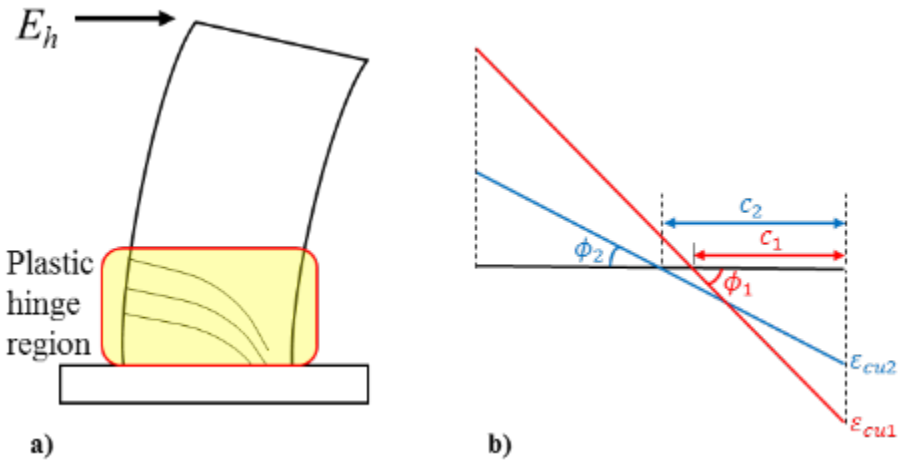

Figure 8. (a) Flexural response of slender wall; and (b) Assumed axial strain distribution in plastic hinge region for two walls with different compression depths

Summary and Conclusions

Valuable experimental data have been generated from recent research conducted to improve the understanding of the seismic performance of thin reinforced concrete structural walls. Isolated boundary element tests provide an economical method for studying the compressive ductility of thin walls sections; however, uniform compressive stress/strain is typically applied to these specimens. Because of the presence of a strain gradient in the compression zone of an actual wall, isolated boundary element tests may under predict the flexural compression capacity of a wall. Test data for three isolated boundary elements and two wall panels were presented, indicating that

the compression strain capacity (at the extreme compression fiber) of a wall is significantly larger than the extreme fiber compression strain capacity measured in an isolated boundary element test. Based on a small set of experimental data, it was shown that curvature plays a role in the compression strain capacity of a wall. As a result, it is suggested that for two walls that are otherwise similar, the compressive strain capacity of a wall with a deeper compression depth (influenced by longitudinal reinforcement, axial load, and cross-section shape) will be smaller. This is particularly important given the fact that the lateral drift ratios allowed by current building codes do not discern differences in the compression demands at the boundaries of walls.

Disclaimer

No formal investigation to evaluate potential sources of uncertainty or error, or to calculate correlations between possible sources of error, was included in this study. The question of uncertainties in the material properties and as-built dimensions are beyond the scope of the work reported here.

References

[1] C. L. Segura, J. W. Wallace, C. A. Arteta, and J. P. Moehle, "Deformation capacity of thin reinforced concrete shear walls," in *Proceedings of 2016 NZSEE Conference*, Auckland, 2016.

[2] A. Rosso, J. P. Almeida, and K. Beyer, "Stability of thin reinforced concrete walls under cyclic loads: state-of-the-art and new experimental findings," (in English), *Bulletin of Earthquake Engineering*, vol. 14, no. 2, pp. 455-484, Feb 2015.

[3] C. A. Arteta, D. V. To, and J. P. Moehle, "Experimental response of boundary elements of code-compliant reinforced concrete shear walls," in *10th US National Conference on Earthquake Engineering, Earthquake Engineering Research Institute*, Anchorage, AK, 2014, vol. 10, no. 4231, p. D37H1DN29.

[4] L. M. Massone, P. Polanco, and P. Herrera, "Experimental and analytical response of RC wall boundary elements," in *10th US National Conference on Earthquake Engineering, Earthquake Engineering Research Institute*, Anchorage, AK, 2014.

[5] T. S. Welt, L. M. Massone, J. M. LaFave, D. E. Lehman, S. L. McCabe, and P. Polanco, "Confinement Behavior of Rectangular Reinforced Concrete Prisms Simulating Wall Boundary Elements," (in English), *Journal of Structural Engineering*, vol. 143, no. 4, p. 04016204, Apr 2017.

[6] ASTM A1064/A1064M-17 (2017), "Standard Specification for Carbon-Steel Wire and Welded Wire Reinforcement, Plain and Deformed, for Concrete," ASTM International, West Conshohocken, PA.

[7] ASTM A706/A706M-16 (2016), "Standard Specification for Low-Alloy Steel Deformed and Plain Bars for Concrete Reinforcement," ASTM International, West Conshohocken, PA.

[8] ACI Committee 318 (2011), "Building Code Requirements for Structural Concrete (ACI 318-11) and Commentary," American Concrete Institute, Farmington Hills, MI.

[9] ACI Committee 318 (2014), "Building Code Requirements for Structural Concrete (ACI 318-14) and Commentary," American Concrete Institute, Farmington Hills, MI.

[10] J. B. Mander, M. J. N. Priestley, and R. Park, "Theoretical Stress-Strain Model for Confined Concrete," (in English), *Journal of Structural Engineering*, vol. 114, no. 8, pp. 1804-1826, Aug 1988.